energies

MDPI

Article

A Novel Approach to Enhancing the Determination of Primary Indicators in Non-Idealised Absorption Chillers

Gábor L. Szabó

Department of Building Services and Building Engineering, Faculty of Engineering, University of Debrecen, Ótemető Str. 2-4, 4028 Debrecen, Hungary; l.szabo.gabor@eng.unideb.hu

Abstract: The accurate optimisation of absorption chillers is often impeded by idealised models that overlook system interactions and machine complexities. This study introduces a validated mathematical description for predicting the primary indicators of non-idealised absorption chillers, accounting for factors such as the electrical work of the Solution Circulation Pump, entropy changes within the refrigerant cycle, and exergy losses. Validation against 13 years of data (2008–2021) from the University of Debrecen's absorption chiller indicated close agreement, with deviations within acceptable limits. The use of a solution heat exchanger shifted cooling indicators towards their minima. Sensitivity analyses indicated that a 2.5% reduction in condenser temperature increased COP by 41.3% and Cooling Exergetic Efficiency by 15.5%, while a 2.5% reduction in the Heat Fraction Factor improved both by 34%. Adjusting absorber temperature and Heat Fraction Factor down by 2.5%, alongside a 2.5% rise in generator temperature, resulted in a 100.8% increase in COP and a 52.8% boost in Cooling Exergetic Efficiency. These insights provide a solid foundation for future optimisation strategies in real-life absorption chiller systems.

Keywords: absorption machine; primary indicators; non-idealised heat pump

Citation: L. Szabó, G. A Novel Approach to Enhancing the Determination of Primary Indicators in Non-Idealised Absorption Chillers. *Energies* **2024**, *17*, 4858. https://doi.org/10.3390/en17194858

Academic Editor: Angelo Maiorino

Received: 30 August 2024
Revised: 24 September 2024
Accepted: 25 September 2024
Published: 27 September 2024

1. Introduction

In recent decades, the role of cooling within the energy balance of buildings has become increasingly critical, largely due to global warming [1]. This trend varies across countries, influenced by factors such as differences in radiative heat gains [2] and specific comfort standards [3]. Meeting the European Union's 2050 Energy Roadmap target of reducing greenhouse gas emissions by 80% compared to 1990 levels [4] has driven the demand for more environmentally friendly and energy-efficient cooling systems across industries [5], transportation, and construction [6]. Of course, the focus should not solely be on energy efficiency and environmental friendliness. In buildings with high human activity, additional viewpoints such as virus risk reduction [7] or ensuring suitable comfort and discomfort levels [8] often dominate. Considering these aspects, too, researchers are focusing on developing systems that offer high energy savings and stability from physical and engineering perspectives while having minimal environmental impact [9,10].

One potential solution for saving energy and reducing annual greenhouse gas emissions is the application of absorption machines. Absorption machines (e.g., chillers and heat pumps) can provide a promising and attractive technology for cooling and even heating functions [11], especially when low- or medium-temperature primary heat sources (for example, geothermal energy [12,13] or solar energy [14,15]) or even secondary energy sources (e.g., waste heat [16,17]) are available. These systems can mitigate the environmental impacts of CO_2 emissions and may contribute to energy savings. The positive effects of absorption machines are primarily due to this [18].

These devices can be categorised based on several criteria, such as the working fluids used (e.g., LiBr-H_2O, H_2O-NH_3), the number of compression stages, the firing method

(indirect or direct), or the temperature of the produced fluid (absorption heat pump or absorption heat transformer) [19,20]. An absorption heat transformer focuses on generating a higher-temperature fluid, while absorption heat pumps concentrate on lower-temperature ones. In recent years, several researchers have examined the industrial applicability of absorption heat pumps for energy-efficient recovery and pollution reduction [21,22]. It is important to note that these machines have a lower coefficient of performance than vapour compression machines. Recent studies on vapour compression systems have reported COPs ranging from 2.5 to 4.7 for various applications. For example, Trutassanawin et al. [23] reported COPs ranging from 2.8 to 4.7 for miniature-scale refrigeration systems, whilst Konovalov et al. [24] achieved a COP value of 7 (at 6 °C coolant temperature) when optimising a low-temperature three-circuit evaporative cooling system for an electric motor using refrigerants. In contrast, absorption systems typically achieve COPs between 0.7 and 0.85; for instance, Manu and Chandrashekar [25] simulated a LiBr absorption heat pump that yielded a COP ranging from 0.7145 to 0.8421 depending on chip temperature. Additionally, Chiriac and Chiriac [26] constructed an analytical model for a water–ammonia solution, achieving a maximum COP of 0.73. Despite this efficiency gap, absorption machines offer unique advantages in certain scenarios. They can utilise low-grade heat sources, operate with environmentally friendly refrigerants, and provide quieter operation, making them particularly suitable for applications where waste heat is available or where environmental concerns are paramount. The development principles of absorption cycles have been widely discussed, e.g., by Wu et al. [27] and Yang et al. [28], with findings applicable in both residential buildings and industrial sectors. An essential development direction is the combination of these systems with other (cooling) technologies to create poly-generation systems. For instance, Toghyani et al. [29] suggested a complex system including a three-stage absorption chiller, a Rankine cycle, a solar collector, an electrolyser, and thermal energy storage for hydrogen production and cooling functions. Liu et al. [30] suggested a GECAHP (Gas Engine Compression–Absorption Heat Pump) system in low air temperatures to improve heating capacity.

Of course, there are numerous articles regarding the optimisation of these systems. For example, Lostec et al. [31] evaluated by experimentation the performance of an absorption chiller, given the changes in various parameters. They found that the performance significantly drops with a decrease in evaporator temperature, attributed to partial evaporation issues when the machine was not operating in its design or nominal state. They also concluded that rich solution flow rate, cooling temperature, and heat source temperature impact the performance. Recent studies have also focused on developing more accurate theoretical models for absorption cycles, addressing the limitations of existing models and exploring the differences between ideal and real absorption cycles [32]. Additionally, novel optimization approaches, such as the heat current method, have been proposed to maximize the cooling capacity of absorption chillers under various operating conditions [33]. The most common method is using one-objective optimisation to minimise or maximise a single parameter. For example, Chen et al. [34] maximised the COP value of an NH_3–H_2O absorption machine by using one-objective optimisation. Although the main results of these optimisation procedures are correct, their precision needs to increase. These studies often start from an idealised description model, focusing on the complex state properties of thermodynamic systems (e.g., cooling cycles), and either entirely or partially ignore the dynamic behaviour observed in real-life operations. For more accurate optimisation, the effects of connected systems and the external and internal irreversibilities of the absorption machine must be considered.

The operation of real-life absorption machines and their connecting systems results in internal and external irreversibilities, which can significantly reduce the performance of the systems. Various optimisation studies have attempted to overcome these irreversibilities using what is referred to as irreversible models [35,36]. For example, Bhardwaj et al. [37] found that internal irreversibilities significantly influence usable performance and differ substantially from external irreversibilities. Furthermore, Qin et al. [38]

demonstrated that the heat capacity values of the components, internal irreversibilities, and external irreversibilities determine the usable performance of absorption heat pumps. Experimental results from Cardoso-Fernandez et al. [39] show that the temperatures of fluids entering and exiting connected systems can significantly affect the Generator–Absorber exchange process. Fumagalli et al. [40] analysed the operation of the Generator–Absorber–Heat Exchanger and showed that the system's performance depends not only on its performance but also on the integration of the machine into the overall power generation system. Browne and Bansal [41] concluded that ignoring the dynamic behaviour frequently observed in real-life operations is unacceptable and inaccurate from a certainty perspective. Therefore, studies on absorption systems should consider, in addition to optimisation, the extent to which the system's usable performance and which components' optimisation can produce the most significant improvement [19].

To optimise absorption machines effectively, it is vital to transcend idealised models and incorporate real-life factors that significantly influence primary performance indicators. This study seeks to refine existing models by addressing key aspects often overlooked in simplified descriptions, including the following:

- The electrical work of the Solution Circulation Pump;
- Entropy loss due to the Expansion Valves before the Evaporator and Absorber;
- Entropy changes resulting from superheating after the Evaporator and subcooling after the Condenser;
- Heat exchange between the machine components and the environment;
- Exergy losses associated with heat losses;
- Exergy destruction within the machine;
- The effects of the Solution Heat Exchanger.

Building on my previous research [42–45], this study introduces a refined approach for more accurate determination of primary indicators in non-idealised absorption chillers, validated using empirical data from a real-life absorption chiller. The contributions of this study include the development of novelty equations for primary indicators and a deeper understanding of system component interactions, providing a solid foundation for both quantitative and qualitative optimisation strategies in real-life absorption chiller systems.

2. Material and Methods

Firstly, compare the schemas of the idealised (Figure 1a) and non-idealised (Figure 1b) absorption chillers, focusing on the energy flows and the operating temperatures.

The operation of the system, as illustrated in Figure 1b, is as follows (the values provided in parentheses enhance clarity and are derived from the data in Table 1): In the Evaporator (T_0 = 7.3 °C), the refrigerant extracts heat from the Chilled Water (from $T_{c,1}$ = 14.0 °C to $T_{c,2}$ = 8.0 °C), causing it to fully evaporate and become superheated. The superheated refrigerant enters the Absorber (T_A = 27.0 °C), where it is absorbed by the Weak Solution, forming the Strong Solution. The heat released during absorption is removed by the Cooling Water (from $T_{h,1}$ = 29.8 °C to $T_{h,3}$ = 28.0 °C). The Strong Solution is pumped through a Solution Heat Exchanger (SHX) to the Generator by the Solution Circulation Pump. There, the Strong Solution is preheated by the Weak Solution returning from the Generator. In the Generator (T_G = 68.4 °C), heat (from $T_{g,1}$ = 85.0 °C to $T_{g,2}$ = 70.0 °C) is applied, causing the refrigerant to separate from the solution, leaving behind a Weak Solution. The Weak Solution flows back to the Absorber via the SHX and an Expansion Valve. The refrigerant, now gaseous, moves from the Generator to the Condenser (T_C = 34.0 °C), where it releases heat to the Chilled Water (from $T_{h,3}$ = 28.0 °C to $T_{h,2}$ = 26.0 °C) from the Absorber, causing it to condense and subcool. Finally, the refrigerant flows back to the Evaporator through an Expansion Valve, completing the cycle.

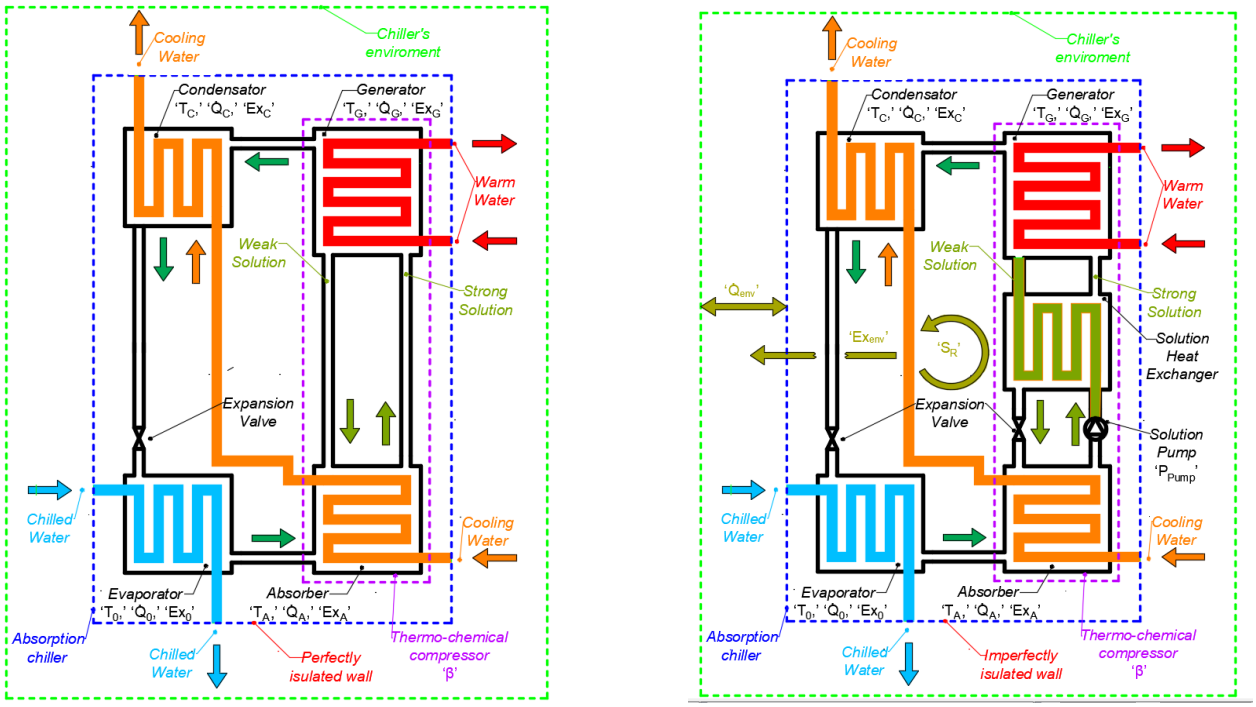

Figure 1. (**a**) Schema of an idealised absorption machine. (**b**) Schema of a non-idealised absorption machine.

Applying Figure 1b, the energy flow (Equation (1)), entropy (Equation (2)), and exergy (Equation (3)) balancing equations can be given for the absorption machines.

$$\dot{Q}_0 + \dot{Q}_G + P_{Pump} = \dot{Q}_A + \dot{Q}_C + \dot{Q}_{env};\ [\mathrm{W}] \tag{1}$$

$$\frac{\dot{Q}_0}{T_0} + \frac{\dot{Q}_G}{T_G} = \frac{\dot{Q}_A}{T_A} + \frac{\dot{Q}_C}{T_C} + S_R;\ \left[\frac{\mathrm{W}}{\mathrm{K}}\right] \tag{2}$$

$$Ex_G + P_{Pump} = Ex_0 + Ex_A + Ex_C + Ex_{env};\ [\mathrm{W}] \tag{3}$$

where '$\dot{Q}_0$' is the cooling capacity; '$\dot{Q}_G$' is the heat consumed in the Generator; 'P_{Pump}' is the electric power consumed by the Solution Circulation Pump; '$\dot{Q}_A$' is the heat released in the Absorber; '$\dot{Q}_C$' is the heat released in the Condenser; and '$\dot{Q}_{env}$' is the heat exchange between parts of the machine and the environment (which can take both positive and negative values; it is considered positive when heat flows from the machine to the environment), all in watts ('W'). 'Ex_0' is the exergy content of '$\dot{Q}_0$'; 'Ex_A' is the exergy content of '$\dot{Q}_A$'; 'Ex_C' is the exergy content of '$\dot{Q}_C$'; 'Ex_G' is the exergy content of '$\dot{Q}_G$'; and 'Ex_{env}' is the difference in the exergy content, all in watts ('W'). 'T_0' is the evaporation temperature; 'T_A' is the absorption temperature; 'T_C' is the condensation temperature; and 'T_G' is the generator temperature, all in kelvins ('K'). 'S_R' is the generated entropy within the refrigerant cycle in watts per kelvin ('$W \cdot K^{-1}$').

The role of the Solution Heat Exchanger is considered essential to highlight here. The impact of the Solution Heat Exchanger is reflected indirectly in the balance equations; it can be observed in the values of the individual energy flows. The primary goal of employing the Solution Heat Exchanger is ensuring that the weak solution entering the Absorber is as cold as possible while the strong solution entering the Generator is as warm as possible. Achieving this goal leads to using much of the heat released in the Absorber within the machine itself rather than requiring its removal. In a non-idealised machine, the value of $\dot{Q}_A$ is expected to be lower than that predicted by models of idealised machines.

The qualitative and quantitative indicators of absorption chillers were derived by using balancing equations. In this article, these indicators (Coefficient of Performance, Thermo-Chemical Efficiency, Exergetic Efficiency, and Exergetic Thermo-Chemical Efficiency) are called primary indicators of absorption machines.

The definition of the cooling and heating Coefficient of Performance is the ratio of the usable cooling and heating energy flow to the introduced energy flow. Its determination is as follows [44,46,47]:

$$COP_C = \frac{\dot{Q}_0}{\dot{Q}_G + P_{Pump}};\ [-] \tag{4}$$

$$COP_H = \frac{\dot{Q}_A + \dot{Q}_C}{\dot{Q}_G + P_{Pump}};\ [-] \tag{5}$$

The cooling and heating Exergetic Efficiency is the ratio of the exergy content of the cooling and heating energy flow to the exergy content of the introduced energy flow [44,46,47]:

$$\eta_{ex,C} = \frac{Ex_0}{Ex_G + P_{Pump}} \cdot 100;\ [\%] \tag{6}$$

$$\eta_{ex,H} = \frac{Ex_A + Ex_C}{Ex_G + P_{Pump}} \cdot 100;\ [\%] \tag{7}$$

After that, two less often applied primary indicators, which represent the ratio of the former primary indicators to their possible maximum, are provided.

The cooling Thermo-Chemical Efficiency compares the cooling Coefficient of Performance to its maximum [44,46,47]:

$$\eta_{A,C} = \frac{COP_C}{COP_{CC}} \cdot 100 \leq 100;\ [\%] \tag{8}$$

where 'COP_{CC}' represents the maximum achievable value of the Coefficient of Performance, as determined by the reverse Carnot cycle.

The cooling Exergetic Thermo-Chemical Efficiency compares the Exergetic Efficiency to its maximum [44]:

$$\eta_{A,ex,C} = \frac{\eta_{ex,C}}{\eta_{ex,max,C}} \cdot 100 \leq 100;\ [\%] \tag{9}$$

where '$\eta_{ex,max,C}$' represents the maximum achievable value of the Cooling Exergetic Efficiency, determined when 'COP_C' equals 'COP_{CC}', in %.

From the viewpoint of the primary indicators, there is no difference between the idealised and the non-idealised absorption chiller. The differences can only be observed if the primary indicators are written down using the secondary indicators. In my previous research [42,43,45,48], these secondary indicators provided deeper information to understand the attributes of the absorption machine. These secondary indicators (Thermo-Chemical Performance Index [42,48], Coefficient Of Compensation For Entropy-Surplus [45], and Thermo-Chemical Instability Index [43]) can be adapted to the non-idealised absorption chiller.

The Thermo-Chemical Performance Index is the ratio of energy flows extracted from and supplied to the Thermo-Chemical Compressor. This secondary indicator characterizes the energy relations of the Thermo-Chemical Compressor [42]:

$$0 \leq \beta = \frac{\dot{Q}_A}{\dot{Q}_G + P_{Pump}};\ [-] \tag{10}$$

Since the heat flow released in the Absorber cannot be negative (not heating the Absorber), this ratio will not be less than zero. This index appears to be an essential indicator of the efficiency of the Solution Heat Exchanger. Because the Solution Heat Exchanger is

more energetically efficient, the Thermo-Chemical Performance Index will be lower. Although the maximum value of this index can be used for the idealised absorption chiller, for the real-life absorption chiller, it can cause more issues than it can resolve.

The Coefficient Of Compensation For Entropy-Surplus is, by definition, the ratio of the generated entropy within the refrigerant cycle and the introduced energy flow [45]:

$$\delta_A = \frac{S_R}{\dot{Q}_G + P_{Pump}};\ \left[\frac{1}{\mathrm{K}}\right] \tag{11}$$

The Thermo-Chemical Instability Index characterizes the exposure of primary indicators to fluctuations in heat sources, as determined by the following equation [43]:

$$0 \le \mu = \frac{J_{max} - J_{min}}{J_{max}} \le 1;\ [-] \tag{12}$$

where 'J_{max}' is the maximum value of the examined primary indicator; and 'J_{min}' is the value of the examined primary indicator when $\beta = 0$.

In the following, the equations of the two most essential primary indicators are provided, along with the previously mentioned secondary indicators, starting from the three balance equations (Equations (1)–(3)):

$$COP_C = \frac{T_0}{T_A} \cdot \frac{T_C - T_A}{T_C - T_0} \cdot \beta + \left[1 + T_C \cdot \delta_A - \frac{\dot{Q}_{env}}{\dot{Q}_G + P_{Pump}} - \frac{\dot{Q}_G}{\dot{Q}_G + P_{Pump}} \cdot \frac{T_C}{T_G}\right] \cdot \frac{T_0}{T_C - T_0}\ ;[-] \tag{13}$$

$$\eta_{ex,C} = \frac{T_G}{T_A} \cdot \frac{T_C - T_A}{T_C - T_0} \cdot \frac{T_X - T_0}{T_G - \frac{\dot{Q}_G}{\dot{Q}_G + P_{Pump}} \cdot T_X} \cdot \beta \cdot 100 + \left[1 + T_C \cdot \delta_A - \frac{\dot{Q}_{env}}{\dot{Q}_G + P_{Pump}} - \frac{\dot{Q}_G}{\dot{Q}_G + P_{Pump}} \cdot \frac{T_C}{T_G}\right] \cdot \frac{T_G}{T_C - T_0} \cdot \frac{T_X - T_0}{T_G - \frac{\dot{Q}_G}{\dot{Q}_G + P_{Pump}} \cdot T_X} \cdot 100;\ [\%] \tag{14}$$

where 'T_X' is the reference temperature, in kelvins ('K').

Since these shapes of the equations did not approach the transparent forms of the idealised absorption chiller [44], further investigation was needed.

3. Results

3.1. New Secondary Indicators

After the theoretical overview, it seemed necessary to introduce three new secondary indicators to facilitate the description of real-life machines. Firstly, the Quality Loss Index ('σ_A') as a secondary indicator is introduced:

$$0 \le \sigma_A = \frac{Ex_{env}}{\dot{Q}_G + P_{Pump}};\ [-] \tag{15}$$

Since exergy can be non-negative, this value will be greater than zero.

Introducing, in addition, the Heat Fraction Factor ('γ'), which gives the part of the heat in the introduced energy flow:

$$0 \le \gamma = \frac{\dot{Q}_G}{\dot{Q}_G + P_{Pump}} \le 1;\ [-] \tag{16}$$

Since Q_G and P_{Pump} can be non-negative, this indicator can vary between 0 and 1.

The third new secondary indicator, the Extreme Values Proximity Index ('λ_C'), can describe how closely the respective indicator can approach its possible maximum and minimum value:

$$0 \le \lambda_C = \frac{J - J_{min}}{J_{max} - J_{min}} \le 1;\ [-] \tag{17}$$

If $\lambda_C = 0.5$, then the indicator is the arithmetic mean of the minimum and maximum values. The investigated indicator is closer to the minimum value when $0.5 > \lambda_C > 0$ while it is closer to the maximum when $0.5 < \lambda_C < 1$.

Henceforth, β, δ_A, σ_A, and γ (i.e., where dividing by the introduced energy flow) are called 'simple secondary indicators,' while μ_C and λ_C are called 'complex secondary indicators.'

If the primary indicators are described using the operating temperature and the secondary indicators, the following equations arise:

$$COP_C = \frac{T_0}{T_C - T_0} \cdot \left[\frac{T_C - T_A}{T_A} \cdot \beta + 1 - \sigma_A + (T_C - T_X) \cdot \delta_A - \frac{T_C}{T_G} \cdot \gamma \right];\ [-] \tag{18}$$

$$\eta_{ex,C} = \frac{T_G}{T_C - T_0} \cdot \frac{T_X - T_0}{T_G - \gamma \cdot T_X} \cdot \left[\frac{T_C - T_A}{T_A} \cdot \beta + 1 - \sigma_A + (T_C - T_X) \cdot \delta_A - \frac{T_C}{T_G} \cdot \gamma \right] \cdot 100;\ [\%] \tag{19}$$

$$\eta_{A,C} = \eta_{A,ex,C} = \frac{T_G}{T_G - T_A} \cdot \frac{1}{\gamma} \cdot \left[\frac{T_C - T_A}{T_A} \cdot \beta + 1 - \sigma_A + (T_C - T_X) \cdot \delta_A - \frac{T_C}{T_G} \cdot \gamma \right] \cdot 100;\ [\%] \tag{20}$$

To provide a comprehensive description of the complex secondary indicators, it is essential to specify the maximum values of the primary indicators as well. The reverse Carnot cycle, which represents the most efficient refrigerant cycle, determines the maximum values of the Coefficient of Performance and Exergetic Efficiency. It is crucial to emphasise that for real-life machines, the value of P_{Pump} cannot be assumed to be zero. Consequently, the maximum values of the primary indicators can be expressed as follows:

$$COP_{CC} = \frac{T_0}{T_G} \cdot \frac{T_G - T_A}{T_C - T_0} \cdot \gamma;\ [-] \tag{21}$$

$$\eta_{ex,max,C} = \frac{T_G - T_A}{T_C - T_0} \cdot \frac{T_X - T_0}{T_G - \gamma \cdot T_X} \cdot \gamma \cdot 100;\ [\%] \tag{22}$$

3.2. Connection Using the Balance Equations

The connection between the values considered as loss ($\dot{Q}_{env}$, S_R, and Ex_{env}) can be determined by applying the three balance equations of the real-life machine (Equations (1)–(3)).

$$\frac{\dot{Q}_{env}}{\dot{Q}_G + P_{Pump}} = T_X \cdot \frac{S_R}{\dot{Q}_G + P_{Pump}} + \frac{Ex_{env}}{\dot{Q}_G + P_{Pump}} = T_X \cdot \delta_A + \sigma_A;\ [-] \tag{23}$$

If the heat flow balance equations (Equation (1)) are divided by the introduced energy flows, the connection between the cooling and heating Coefficient of Performance is obtained:

$$COP_H - COP_C = 1 - \frac{\dot{Q}_{env}}{\dot{Q}_G + P_{Pump}} = 1 - T_X \cdot \delta_A - \sigma_A;\ [-] \tag{24}$$

In an idealised absorption chiller, the difference between the heating and cooling Coefficient of Performance is exactly one.

Furthermore, the connection between the heating and cooling Exergetic Efficiency can be obtained if the exergy balancing equation is divided by the exergy contents of the introduced energy flows:

$$\begin{aligned} \eta_{ex,C} + \eta_{ex,H} &= 100 - \frac{Ex_{env}}{Ex_G + P_{Pump}} \cdot 100 \\ &= 100 - \sigma_A \cdot \frac{T_G}{T_G - \gamma \cdot T_X} \cdot 100;\ [\%] \end{aligned} \tag{25}$$

In idealised machines, the sum of the heating and cooling Exergetic Efficiency is exactly 100%.

3.3. A Novelty Description of the Primary Indicators

Because of the effect of the Solution Heat Exchanger (contrary to my previous research), the value of primary indicators should not be based on their maximum value. When the Solution Heat Exchanger operates in a theoretically perfect manner, the heat released in the Absorber (Q_A) does not need to be removed by the Cooling Water. In this idealised scenario, the Solution Heat Exchanger effectiveness ensures that Q_A is exactly zero, and consequently, the Thermo-Chemical Performance Index is also zero. Consider this case as the minimum value of the primary indicators occurring theoretically during the actual operation of the absorption machine (their absolute minimum value is, of course, zero, but then the machine's operation is stopped):

$$COP_{min,C} = \frac{T_0}{T_C - T_0} \cdot \left[1 - \sigma_A + (T_C - T_X) \cdot \delta_A - \frac{T_C}{T_G} \cdot \gamma\right];\ [-] \tag{26}$$

$$\eta_{ex,min,C} = \frac{T_G}{T_C - T_0} \cdot \frac{T_X - T_0}{T_G - \gamma \cdot T_X} \cdot \left[1 - \sigma_A + (T_C - T_X) \cdot \delta_A - \frac{T_C}{T_G} \cdot \gamma\right] \cdot 100;\ [\%] \tag{27}$$

$$\begin{aligned} \eta_{A,min,C} &= \eta_{A,ex,min,C} \\ &= \frac{T_G}{T_G - T_A} \cdot \frac{1}{\gamma} \cdot \left[1 - \sigma_A + (T_C - T_X) \cdot \delta_A - \frac{T_C}{T_G} \cdot \gamma\right] \cdot 100;\ [\%] \end{aligned} \tag{28}$$

As observed, the values of Thermo-Chemical Efficiency and Exergetic Thermo-Chemical Efficiency coincide.

The application of the Solution Heat Exchanger, therefore, brings the primary indicators closer to their minimum values. Therefore, when formulating the primary indicators, it is advisable to utilise the complex secondary indicators, which characterise the relationship between the maximum and minimum values. As an initial step, let us express the complex secondary indicators in terms of the operating temperature and the simple secondary indicators. To achieve this, we shall employ the relationships established in Equations (21) and (22) and Equations (26)–(28). Firstly, the Extreme Values Proximity Index is:

$$\begin{aligned} \lambda_C &= \frac{COP_C - COP_{min,C}}{COP_{CC} - COP_{min,C}} = \frac{\eta_{ex,C} - \eta_{ex,min,C}}{\eta_{ex,max,C} - \eta_{ex,min,C}} = \frac{\eta_{A,C} - \eta_{A,min,C}}{100 - \eta_{A,min,C}} \\ &= \frac{\eta_{A,ex,C} - \eta_{A,ex,min,C}}{100 - \eta_{A,ex,min,C}} \end{aligned} \tag{29a}$$

$$\lambda_C = \frac{T_C - T_A}{T_A \cdot \left[\frac{T_G - T_A + T_C}{T_G} \cdot \gamma - 1 + \sigma_A - (T_C - T_X) \cdot \delta_A\right]} \cdot \beta -; \ [-] \tag{29b}$$

Secondary, the Thermo-Chemical Instability Index of the primary indicators in real-life machines by the extreme values:

$$\mu_C = \frac{COP_{CC} - COP_{min,C}}{COP_{CC}} = \frac{\eta_{ex,max,C} - \eta_{ex,min,C}}{\eta_{ex,max,C}} = \frac{1 - \eta_{A,min,C}}{1} = \frac{1 - \eta_{A,ex,min,C}}{1}; \ [-] \tag{30a}$$

$$\mu_C = \frac{T_G}{T_A} \cdot \frac{T_C - T_A}{T_G - T_A} \cdot \frac{\beta}{\gamma \cdot \lambda_C}; \ [-] \tag{30b}$$

Using the presented equations, the primary indicators of real-life absorption machines can be expressed with their extreme values and the (complex) secondary indicators as follows:

$$COP_C = COP_{min,C} \cdot \left[1 + \frac{\mu_C}{1 - \mu_C} \cdot \lambda_C\right]; \ [-] \tag{31}$$

$$\eta_{ex,C} = \eta_{ex,min,C} \cdot \left[1 + \frac{\mu_C}{1 - \mu_C} \cdot \lambda_C\right]; \ [\%] \tag{32}$$

$$\eta_{A,C} = \eta_{A,ex,C} = \eta_{A,ex,min,C} + \mu_C \cdot \lambda_C \cdot 100 = \eta_{A,min,C} + \mu_C \cdot \lambda_C \cdot 100; \ [\%] \tag{33}$$

Thus, it is possible to express the primary indicators with their minimum values, requiring only the application of the two complex secondary indicators. Interestingly, the ratio of the two most important primary indicators to their minimum values is identical. This relationship is not immediately apparent from either Equations (13) and (14) or Equations (18)–(22).

4. Validation

The measured data from a real-life machine were used to validate the results. This absorption chiller is located at the Medical Centre of the University of Debrecen. This machine is inspected for maintenance twice yearly (at the beginning and end of the cooling season). The measurements are conducted by Johnson Controls. Primarily, the measurements focus on examining the operational ability of the machine, thus providing data on the temperatures of the cooling water, chilled water, and warm water for the entire operational period (8 April 2008–24 May 2022). During the inspection, there is an opportunity to measure the internal temperatures as well, at an auditor's decision. Unfortunately, this was not consistently performed in each case, resulting in only 14 usable datasets out of the available 29 for validation. These 14 values are evenly distributed over the operational period (see later in Table 2).

The data of the examined machine (York YIA-HW-6C4-50) in its design state are summarized in Table 1. The connected secondary systems of this absorption chiller operate with constant volume flow rate pumps.

Table 1. The main data of the real-life machines.

Denomination	Notation	Value
Energy flow	$\dot{Q}_0/\dot{Q}_G/P_{pump}/\dot{Q}_H$; in kW	910/1312.5/15.8/2154.6
	$\dot{Q}_A/\dot{Q}_C/\dot{Q}_{env}$; in kW	1134.0/1020.6/83.7
Exergy	$Ex_0/Ex_G/P_{pump}$; in kW	60.68/162.93/15.8
	$Ex_A/Ex_C/Ex_{env}$; in kW	3.78/26.58/87.66
Temperature	T_0/ T_C; in °C	7.3/34.0
	T_A/T_G; in °C	27.0/68.4

	$T_{c,1}/T_{c,2}$; in °C	14.0/8.0
	$T_{g,1}/T_{g,2}$; in °C	85.0/70.0
	$T_{h,1}/T_{h,2}$; in °C	29.8/26.0
	T_X; in °C	26.0
Volume flow	$\dot{V}_{chilled}$; in m³/h (at the Evaporator)	130
	$\dot{V}_{cooling}$; in m³/h (at the Absorber and the Condenser)	486
	$\dot{V}_{warm}$; in m³/h (at the Generator)	75
Simple secondary indicators	β	0.864
	δ_A	−0.00001006
	σ_A	0.06599
	γ	0.9881
Complex secondary indicators	μ_C	0.6217
	λ_C	0.2674
Primary indicators	COP_C/COP_H	0.685/1.622
	$\eta_{ex,C}/\eta_{ex,H}$; in %	33.96/16.99
	$\eta_{A,C}/\eta_{A,ex,C}$; in %	54.46/54.46

The measured values are shown in Figure 2.

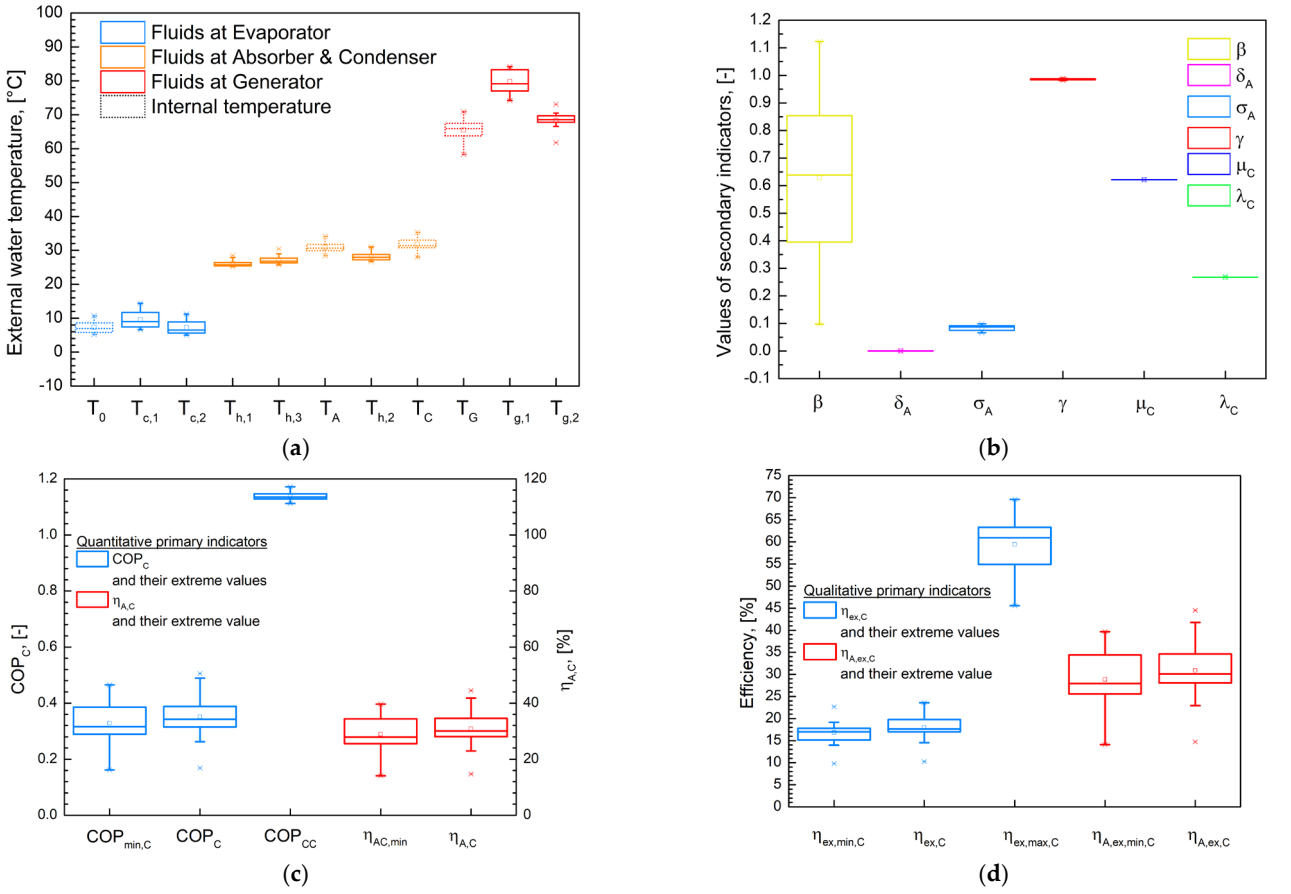

Figure 2. (**a**) The external and internal temperatures; (**b**) secondary indicators; (**c**) energetic primary indicators and their extreme values; and (**d**) exergetic primary indicators and their extreme values.

In Figure 2a, the average standard deviation is 1.85. The temperatures of the generator heating system ($T_{g,1}$ and $T_{g,2}$) exhibit higher standard deviations (exceeding 3), whilst the cooling water system ($T_{h,1}$, $T_{h,3}$, $T_{h,2}$) shows significantly lower values (below 1.18).

However, the latter demonstrates high positive skewness (>+1), whereas $T_{g,1}$ has a skewness of 0.0. Regarding the secondary indicators (Figure 2b), the notable standard deviation of β (0.289, compared to the mean of 0.06) and the skewness of λ_C (+1.41) are particularly noteworthy. For the primary indicators and their extreme values (Figure 2c,d), the average standard deviation is 1.3. This arises from most values being below 1, whilst the (cooling) exergetic efficiency and its extreme values show considerably high standard deviations (exceeding 3). A further point of interest is the substantial skewness in the values of COP_{CC} and $\eta_{ex,max,C}$ (+0.61 and −0.66, respectively).

In Table 2, the difference between the COP_C and $\eta_{ex,C}$ values determined from the measured values (Figure 2c,d) and those determined based on the novelty mathematical description (Equations (18), (19), (31) and (32)) are presented.

Table 2. Deviation between measured and model-determined COP_C and $\eta_{ex,C}$ values.

Date of Measurement	COP_C; [-]			$\eta_{Ex,C}$; [%]		
	Based on Measure Data Equation (4)	Based on Model Equation (18)	Deviation	Based on Measure Data Equation (6)	Based on Model Equation (19)	Deviation
13 May 2021	0.3441	0.3441	$-1.943 \cdot 10^{-15}$	19.778	19.778	$-1.279 \cdot 10^{-13}$
7 September 2020	0.5059	0.5059	$3.664 \cdot 10^{-15}$	20.279	20.279	$9.948 \cdot 10^{-14}$
29 August 2018	0.3147	0.3147	$2.109 \cdot 10^{-15}$	16.986	16.986	$1.101 \cdot 10^{-13}$
5 July 2017	0.3172	0.3172	$-2.165 \cdot 10^{-15}$	17.675	17.675	$-1.279 \cdot 10^{-13}$
27 September 2016	0.1686	0.1686	$2.165 \cdot 10^{-15}$	10.242	10.242	$1.261 \cdot 10^{-13}$
5 July 2016	0.3522	0.3522	$2.665 \cdot 10^{-15}$	16.514	16.514	$1.279 \cdot 10^{-13}$
25 August 2014	0.2625	0.2625	$8.327 \cdot 10^{-16}$	14.523	14.523	$5.684 \cdot 10^{-14}$
10 June 2014	0.3881	0.3881	0	17.533	17.533	0
9 September 2013	0.3404	0.3404	$-6.661 \cdot 10^{-16}$	18.724	18.724	$-4.263 \cdot 10^{-14}$
29 May 2013	0.3209	0.3209	$-3.164 \cdot 10^{-15}$	17.357	17.357	$-1.599 \cdot 10^{-13}$
27 June 2012	0.3637	0.3637	$1.110 \cdot 10^{-15}$	17.653	17.653	$9.237 \cdot 10^{-14}$
21 June 2011	0.4393	0.4393	0	23.584	23.584	0
31 May 2011	0.4897	0.4897	0	22.949	22.949	0
18 July 2008	0.3089	0.3089	$1.998 \cdot 10^{-15}$	17.964	17.964	$1.101 \cdot 10^{-13}$

Based on this table, it can be observed that the model closely follows the measurement results.

The values for the secondary indicators at the designed and operational states are compared in the following. The designed state values are not significantly deviant, excluding the Extreme Values Proximity Index value. This deviant is shown in Figure 3.

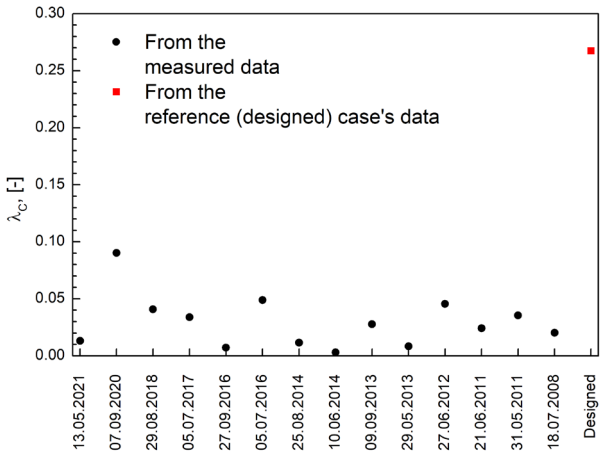

Figure 3. Values of Extreme Values Proximity Index at measurement time points for the examined machine.

From Figure 3, the λ_C value is consistently lower than the design state value in all cases. Therefore, the λ_C value should be advisably maximised in the design state, as it will likely decrease during operation.

5. Discussion

5.1. Correlation and Significance Analysis

Based on the measured results, a correlation and significance analysis were conducted on the connection between the primary indicators and the other factors in the equations. The factors were categorised into three groups for analysis. First, the measured temperatures (Table 3), followed by the extreme values of the primary indicators (Table 4), and finally, the secondary indicators (Table 5) were investigated.

Table 3. Correlation and significance analysis of measured operating temperatures with cooling primary indicators.

	Pearson Correlation			**Significance**		
	COP_C	**$\eta_{ex,C}$**	**$\eta_{A,C}$; $\eta_{A,ex,C}$**	**COP_C**	**$\eta_{ex,C}$**	**$\eta_{A,C}$; $\eta_{A,ex,C}$**
T_0	0.7044	0.33792	0.69137	0.00491	0.23734	0.00617
T_A	0.72665	0.39009	0.7382	0.00324	0.16793	0.00257
T_C	0.58126	0.17606	0.58728	0.02925	0.54713	0.02723
T_G	0.39127	0.11736	0.41068	0.16654	0.68949	0.14467

The values at COP_C, $\eta_{A,C}$, and $\eta_{A,ex,C}$ are similar, while values at $\eta_{ex,C}$ are significantly different. It can be concluded that the $\eta_{ex,C}$ is less dependent on temperature than the other primary indicator. Furthermore, it can also be observed that each primary indicator depends most on the absorption temperature and, to a similar but lesser extent, on the evaporation temperature.

Table 4. Correlation and significance analysis of cooling primary indicators with their extreme values.

	Pearson Correlation			**Significance**		
	COP_C	**$\eta_{ex,C}$**	**$\eta_{A,C}$; $\eta_{A,ex,C}$**	**COP_C**	**$\eta_{ex,C}$**	**$\eta_{A,C}$; $\eta_{A,ex,C}$**
$COP_{min,C}$	0.98373	0.90262	0.98248	0.00000	0.00001	0.00000
COP_{CC}	0.20153	0.09270	0.14440	0.48964	0.75261	0.62235
$\eta_{ex,min,C}$	0.81141	0.97655	0.81359	0.00043	0.00000	0.00040
$\eta_{ex,max,C}$	−0.78042	−0.41638	−0.78365	0.00099	0.13862	0.00091
$\eta_{A,min,C}$; $\eta_{A,ex,min,C}$	0.98091	0.90317	0.98327	0.00000	0.00001	0.00000

According to Table 4 (also Figure 2, naturally), the primary indicators depend most on their minimum values. Surprisingly, the value of COP_C depends little on its maximum value, which is determined by the reverse Carnot cycle (future research can examine the cause of this).

Table 5. Correlation and significance analysis of secondary indicators with cooling primary indicators.

Secondary Indicators		**Pearson Correlation**			**Significance**		
		COP_C	**$\eta_{ex,C}$**	**$\eta_{A,C}$; $\eta_{A,ex,C}$**	**COP_C**	**$\eta_{ex,C}$**	**$\eta_{A,C}$; $\eta_{A,ex,C}$**
Simple	β	0.83736	0.75826	0.83155	0.00019	0.00167	0.00023
	δ_A	−0.55504	−0.48865	−0.54258	0.03937	0.07622	0.04499
	σ_A	−0.91356	−0.75318	−0.90144	0.00000	0.00187	0.00001
	γ	−0.30883	−0.49928	−0.31318	0.28266	0.06912	0.27559
Complex	μ_C	−0.98091	−0.90318	−0.98327	0.00000	0.00001	0.00000
	λ_C	0.58502	0.32680	0.58250	0.02798	0.25410	0.02883

Based on Table 5, among the simple secondary indicators, σ_A (followed by β) relates most closely to primary indicators. This connection is not evident for γ and δ_A. Of the

complex secondary indicators, rather μ_C shows a closer connection with the primary indicators.

5.2. Sensitivity Analysis

The values of the cooling primary indicators are closer to their minimum values when a solution heat exchanger is utilised. This hypothesis is supported by Figure 2c,d and Table 4 as well. Therefore, it is beneficial to examine what influences the minimum values of the primary indicators and determine their sensitivity. These details could be relevant for later optimisation processes in determining intervention points. Furthermore, it is also important to examine whether the primary indicators are as sensitive to changes in a parameter as the extreme values of the same primary indicators. For this analysis, a form of the primary indicators and their minimum values, which are defined by operating temperatures and simple secondary indicators (β, σ_A, δ_A, and γ), was used. (i.e., Equations (18)–(20) and Equations (26)–(28), respectively)

The results of the sensitivity analysis are shown in Figure 4.

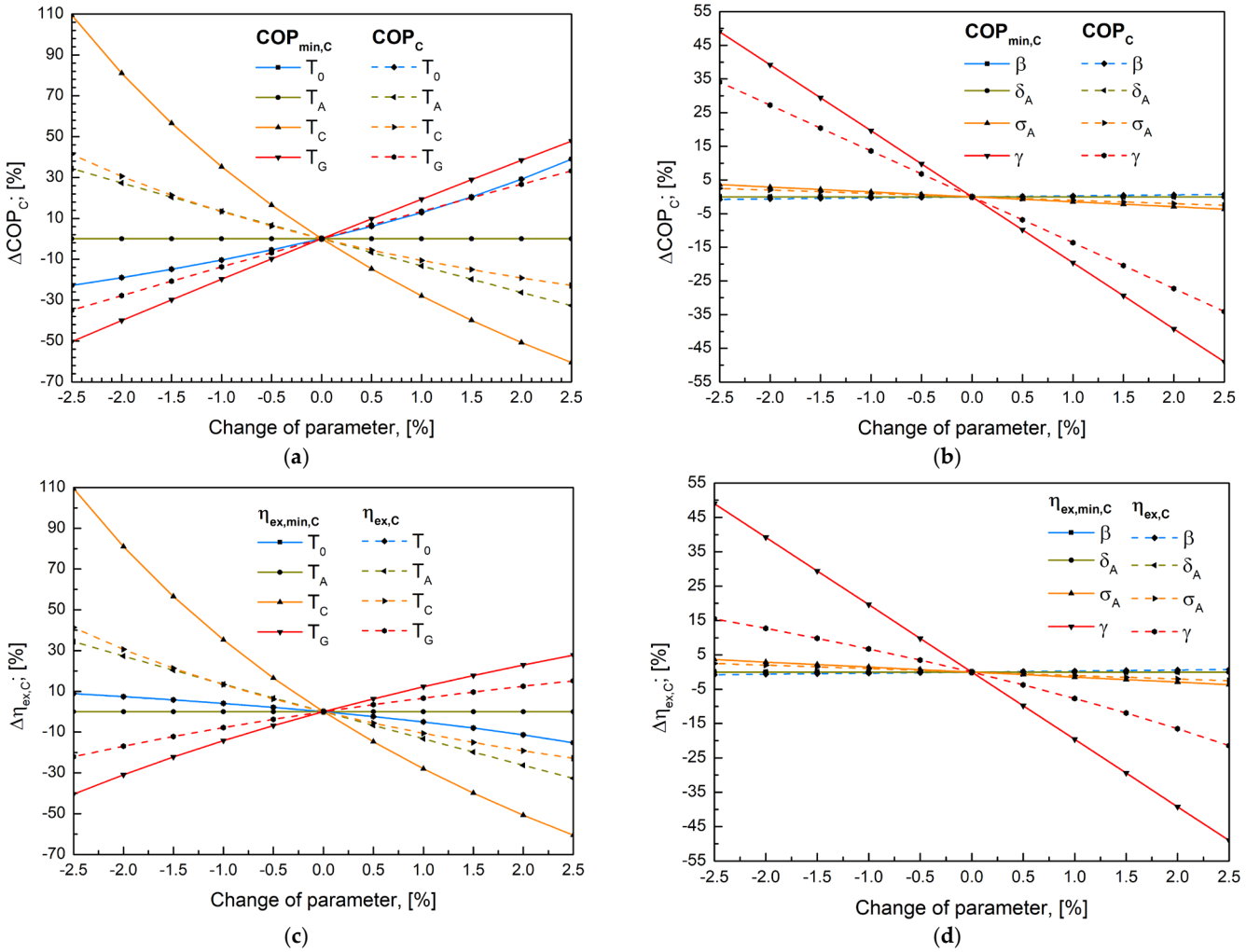

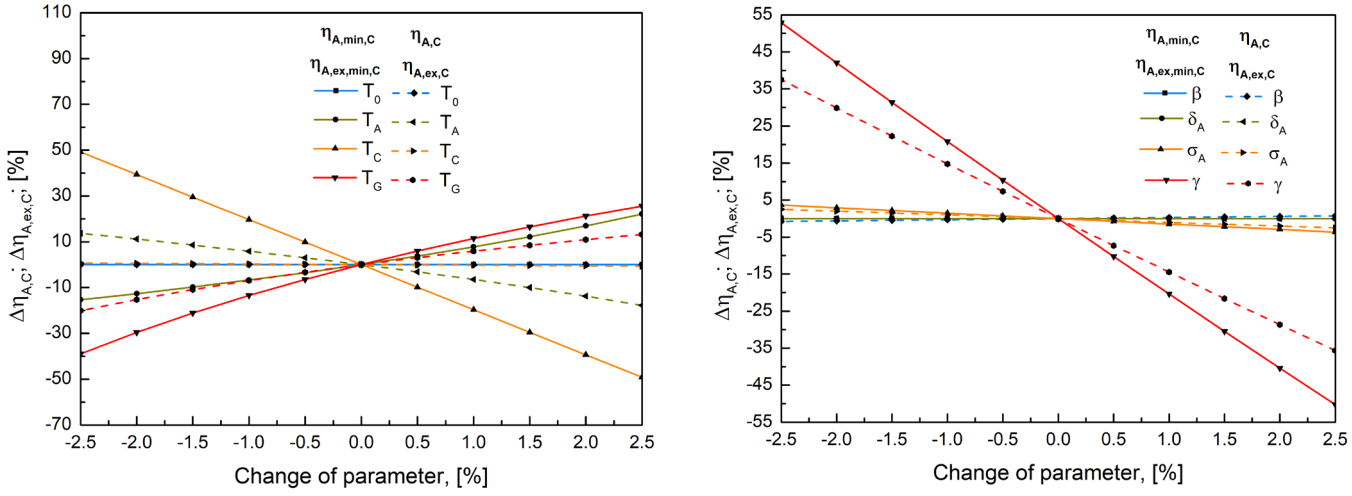

Figure 4. Sensitivity of (**a**) COP_C depending on operating temperatures; (**b**) COP_C depending on secondary indicators; (**c**) $\eta_{ex,C}$ depending on operating temperatures; (**d**) $\eta_{ex,C}$ depending on secondary indicators; (**e**) $\eta_{A,C}$ and $\eta_{A,ex,C}$ depending on operating temperatures; (**f**) $\eta_{A,C}$ and $\eta_{A,ex,C}$ depending on secondary indicators.

Figure 4 shows a complete insensitivity firstly between $\eta_{A,C}$, $\eta_{A,ex,C}$, $\eta_{A,min,C}$, and $\eta_{A,ex,min,C}$ and the evaporation temperature change; secondary between $COP_{min,C}$ and $\eta_{ex,min,C}$ and the absorption temperature change; and finally between the minimum values of the primary indicators ($\eta_{A,min,C}$, $\eta_{A,ex,min,C}$, $COP_{min,C}$, $\eta_{ex,min,C}$) and changes in the Thermo-Chemical Performance Index. Low sensitivity is observed between all examined parameters and changes in the Coefficient of Compensation for Entropy-Surplus, as well as between the primary indicators and changes in the Thermo-Chemical Performance Index. The primary indicators exhibit the same sensitivity to changes in evaporating temperature, as do each of their minimum values. The sensitivity of COP_C and $\eta_{ex,C}$ is the same for changes in the absorption temperature as well as changes in the condensation temperature. The same is found between $COP_{min,C}$ and $\eta_{ex,min,C}$.

Further observations can be made by carefully examining Figure 4. It is noted that T_A, T_C, T_G, and γ have the most significant impact on the values of COP_C and $\eta_{ex,C}$. Additionally, changes in absorption temperature have a similar but contrasting impact on the values of $\eta_{A,C}$ and $\eta_{A,min,C}$. Conversely, changes in the condensation temperature have minimal impact on the values of $\eta_{A,C}$ and $\eta_{A,ex,C}$.

5.3. Analysis of the Convergence of Primary Indicators to Their Maximum Using the Extreme Values Proximity Index

Based on Equation (29b), this complex secondary indicator depends on three operating temperatures (T_A, T_C, and T_G) and four simple secondary indicators (β, σ_A, δ_A, and γ), i.e., seven possible parameters can be varied. The convergence of $\lambda_C = 1$ (i.e., the primary indicators reach their maximum value) by adjusting the values of the reference system (Table 1, $\lambda_C = 0.2674$) by at most 2.5% (similar to the sensitivity analysis) was investigated, considering the extreme values of the secondary indicators. A total of one hundred twenty-seven different cases can be constructed by changing the seven possible parameters. The achievable λ_C values in each case are shown in Figure 5a. Changing λ_C with the possible parameters naturally affects the primary indicators. These effects can be shown in Figure 5b–d.

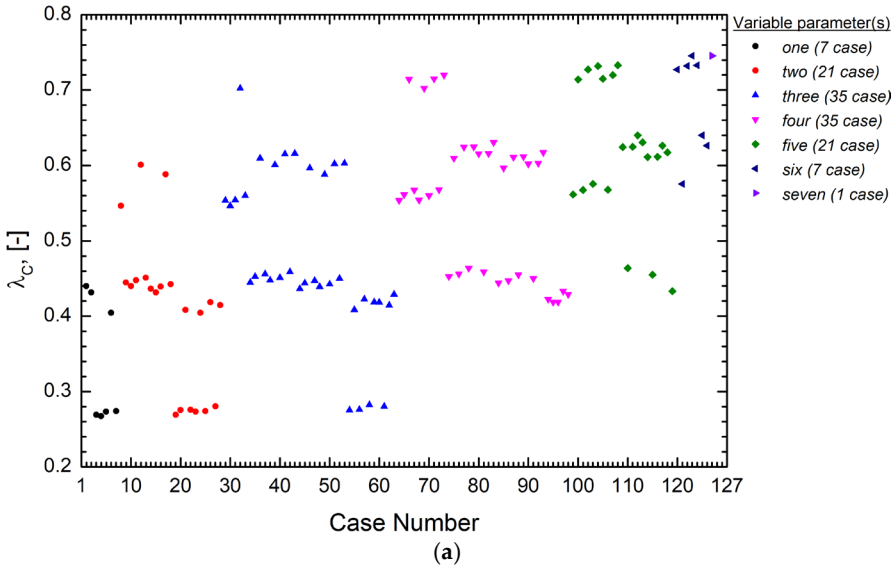
Variable parameter(s)
one (7 case)
two (21 case)
three (35 case)
four (35 case)
five (21 case)
six (7 case)
seven (1 case)
λC, [-]
Case Number

(**a**)

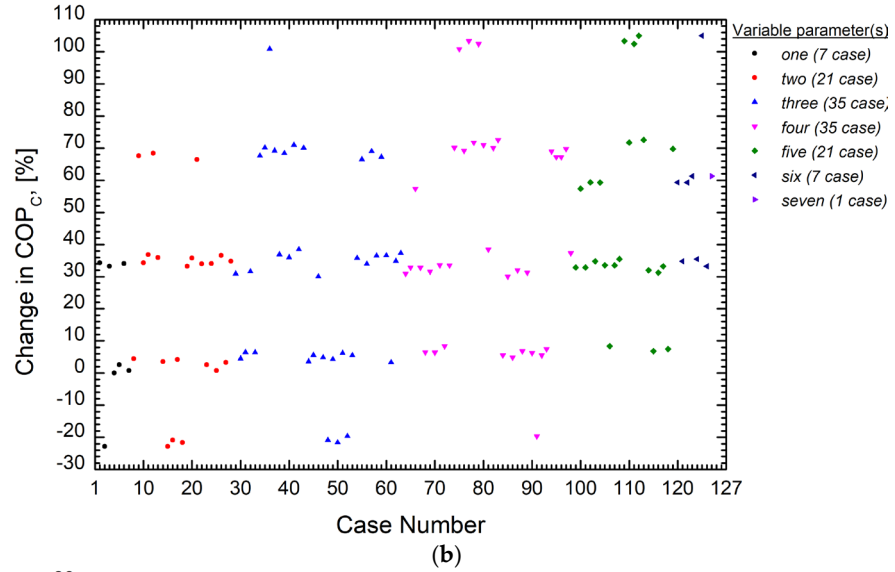
Variable parameter(s)
one (7 case)
two (21 case)
three (35 case)
four (35 case)
five (21 case)
six (7 case)
seven (1 case)
Change in COPC, [%]
Case Number

(**b**)

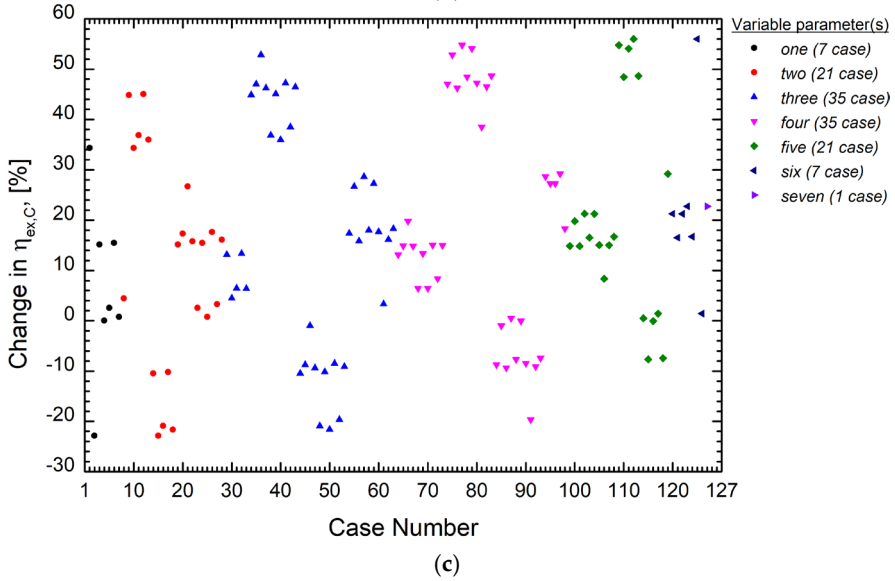
Variable parameter(s)
one (7 case)
two (21 case)
three (35 case)
four (35 case)
five (21 case)
six (7 case)
seven (1 case)
Change in ηex,C, [%]
Case Number

(**c**)

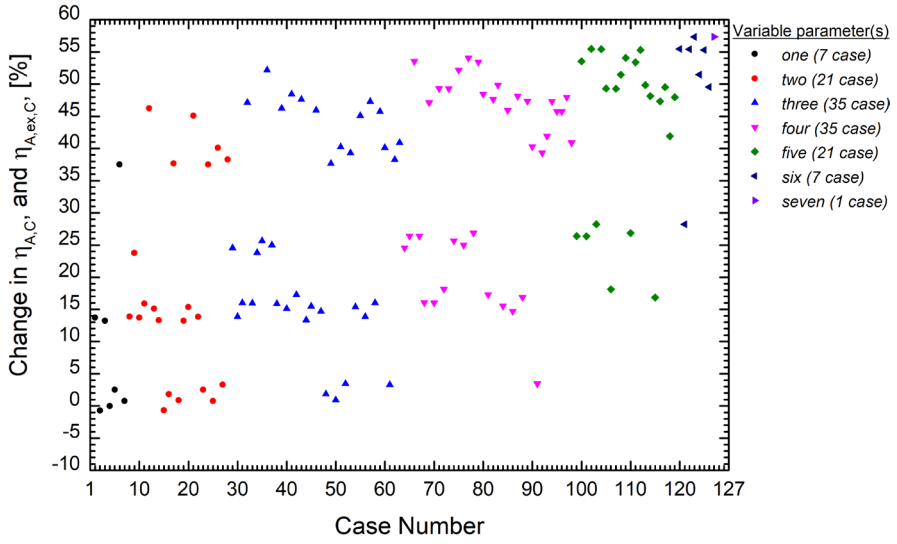

(**d**)

Figure 5. The achievable (**a**) λ_C values (**b**) COP_C changing, (**c**) $\eta_{ex,C}$ changing, (**d**) $\eta_{A,C}$ and $\eta_{A,ex,C}$ changing by adjusting the seven possible parameters.

The $\lambda_C = 1$ can be reached by changing at most 2.5%, based on Figure 5a. It is closest to this value if the varying parameters include T_A, T_C, and γ. Analysing Figure 5b,c,d, groups can be formed among the results based on all three diagrams, although the group boundaries are not perfectly clear and may overlap in some cases. It is evident that the cases involving changes in T_A, T_G, and γ, while keeping T_C constant, consistently produce the best results. These cases (with the number of variables in parameters) are: Case 36 (3); 75 (4); 77 (4); 79 (4); 109 (5); 111 (5); 112 (5); and 125 (6).

Contrary to the λ_C convergence, the highest increase in the value of the primary indicators can be obtained with varying T_A, T_G, and γ if the T_C remains unchanged. If only the values of T_A, T_G, and γ are changed by at most 2.5% (this is Case 36), it increases by 100.8% in COP_C, by 52.84% in $\eta_{ex,C}$, and by 52.14% in $\eta_{A,C}$ and $\eta_{A,ex,C}$. Another interesting result is that changing the T_C value to increase λ_C leads to a decrease in the primary indicators or causes a reduction in the increase caused by T_A, T_G, and γ. Based on these findings, simultaneous decreasing of T_A and γ and increasing of T_G are recommended for optimal performance improvement.

5.4. The Qualitative and Quantitative Nature of Indicators and Their Included Parameters

Effective optimisation and precise control, particularly intervention in problems, require not only precise objective definition but also a clear understanding of how affected characteristics influence other parameters. Without sufficiently detailed knowledge of these interactions, there is a risk of creating a larger problem than the original one. To mitigate this risk, my objective is to thoroughly explore the relationships between operating temperatures and performance-influencing parameters (e.g., secondary indicators), and their effects on primary indicators. This may require understanding how these parameters interact, which characteristics are more or less significant, and whether these parameters predominantly influence quantitative or qualitative aspects of the process.

In my previous article ([44]) a summary diagram illustrated the connections between 'Basic data,' 'Secondary indicators,' and 'Primary indicators' and whether the data represented a predominantly quantitative or qualitative nature. Building on the analyses presented in that article, these connections can be extended to non-idealised systems. These connections are visualised in Figure 6.

The 'Basic data' consists of measured temperatures, while the 'Simple secondary indicators' are defined in Equations (10), (11), (15), and (16). The relationship between 'Basic data' and 'Simple secondary indicators' with the 'Minimum values of primary indicators'

is described in Equations (26)–(28), whereas their connection to 'Complex secondary indicators' is outlined in Equations (29a), (29b), (30a) and (30b). The relationship between 'Primary indicators' and both 'Minimum values of primary indicators' and 'Complex secondary indicators' is defined in Equations (31)–(33).

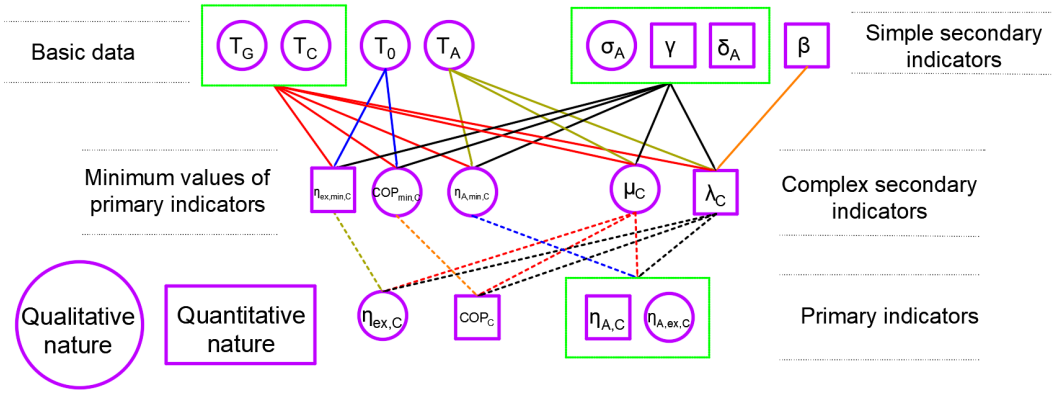

Figure 6. Connections and qualitative/quantitative nature of basic data, secondary indicators, and primary indicators.

When determining the nature of the characteristics, a few factors could be considered purely qualitative or quantitative. A factor was classified as qualitative if its determination required only temperatures ('Basic data') or exergy contents ($\eta_{ex,C}$, $\eta_{A,ex,C}$), and as quantitative if it could be defined as a ratio of heat flows (COP_C, $\eta_{A,C}$, β, and γ). For other factors, the nature was less clear, prompting a closer examination of the strength of their correlation with, and significance related to the temperatures. Therefore, their connections with the operating temperatures are examined in Table 6.

Table 6. Correlation and significance analysis of secondary indicators, and minimum values of cooling primary indicators with operating temperatures.

	Pearson Correlation				**Significance**			
	T_0	**T_A**	**T_C**	**T_G**	**T_0**	**T_A**	**T_C**	**T_G**
σ_A	−0.8067	−0.6367	−0.5747	−0.2155	4.89×10^{-4}	0.0143	0.0316	0.4594
δ_A	−0.2977	−0.3628	−0.2706	−0.3009	0.3013	0.2024	0.3495	0.2959
μ_C	−0.6034	−0.7183	−0.5045	−0.4128	0.0224	0.0038	0.0658	0.1424
λ_C	0.7482	0.4652	0.6628	0.1944	0.00208	0.0937	0.0098	0.5055
$COP_{min,C}$	0.6177	0.7059	0.4985	0.3915	0.0186	0.0048	0.0696	0.1662
$\eta_{EX,min,C}$	0.2108	0.3379	0.0602	0.1053	0.4695	0.2374	0.8381	0.7203
$\eta_{A,min,C}$; $\eta_{A,ex,min,C}$	0.6034	0.7183	0.5045	0.4128	0.0224	0.0038	0.0658	0.1424

The analysis revealed that among the factors with uncertain nature, σ_A is closely related with temperatures, while δ_A and $\eta_{EX,min,C}$ show no significant correlation. As a result, the former was classified as qualitative, while the latter was deemed quantitative. The nature of the remaining four characteristics was not definitively determined based on these analyses, suggesting that further studies and additional measured data should be considered in future research. When constructing the figure, I primarily considered the results of the significance analysis, categorising μ_C, $COP_{min,C}$, and $\eta_{A,min,C}$ ($\eta_{A,ex,min,C}$) as qualitative characteristics, whereas λ_C was regarded as more quantitative in nature.

Understanding these relationships and classifications is essential for identifying intervention points in future optimisation and efficiency improvement processes.

6. Conclusions

Specifically, this study successfully developed and validated a mathematical description of non-idealised absorption machines, incorporating often-overlooked aspects, such as the electrical work of the Solution Circulation Pump, the entropy generated within the refrigerant cycle, and the differences in exergy content. The introduction of secondary indicators, including the Quality Loss Index, Heat Fraction Factor, and Extreme Values Proximity Index, simplifies the representation of complex mathematical relationships and aids in exploring the relationship between primary indicators and their extreme values.

Data from the University of Debrecen's real-life absorption chiller support the description's effectiveness. The validation process indicated that the values of primary indicators approach their minimum values ($\lambda_C < 0.1$) when using the Solution Heat Exchanger. Sensitivity analyses show that small changes in main parameters can lead to substantial performance improvements. For instance, a 2.5% decrease in condenser temperature results in a 41.34% increase in COP_C and a 15.49% increase in $\eta_{ex,C}$, while a 2.5% decrease in the Heat Fraction Factor yields a 34.06% increase in both indicators. Based on the correlation and significance analysis, T_A, T_C, σ_A, and β are of significant importance. Conversely, based on the sensitivity analysis, T_A, T_C, T_G, and γ have the most significant impact on the values of primary indicators. However, the convergence analysis shows that only T_A, T_C, and γ are the most significant in inducing primary indicator values (suggesting that T_G has less impact than the other three indicators). Finally, as a summary of the results, a comprehensive figure is developed to briefly present the indicated connections, highlighting the quantitative or qualitative nature of each parameter.

Given these findings, future research and optimisation strategies should focus on T_A, T_C, and γ, as these parameters have the most significant impact on primary indicator values. The comprehensive analysis presented in this study provides a foundation for enhancing the efficiency and performance of real-life absorption chiller systems, offering both quantitative and qualitative insights to guide future optimisation efforts in this critical area of sustainable cooling technology.

Funding: Project no. TKP2021-NKTA-34 was implemented with the support provided from the National Research, Development and Innovation Fund of Hungary, financed under the TKP2021-NKTA funding scheme.

Data Availability Statement: The original contributions presented in the study are included in the article, further inquiries can be directed to the author.

Conflicts of Interest: The author declares no conflicts of interest.

Nomenclature

Q_0	is the cooling capacity, in W.
Q_A	is the heat released in the Absorber, in W.
Q_C	is the heat released in the Condenser, in W.
Q_G	is the heat consumed in the Generator, in W.
Q_H	is the total heat released in the Absorber and Condenser, in W.
P_{Pump}	is the electric power consumed by the Solution Circulation Pump, in W.
Q_{env}	is the heat exchange between parts of the machine and the environment, in W.
S_R	is the generated entropy within the refrigerant cycle, in $W \cdot K^{-1}$.
Ex_0	is the exergy content of $\dot{Q}_0$, in W.
Ex_A	is the exergy content of $\dot{Q}_A$, in W.
Ex_C	is the exergy content of $\dot{Q}_C$, in W.
Ex_G	is the exergy content of $\dot{Q}_G$, in W.
Ex_{env}	is the difference in the exergy contents, in W.
T_0	is the evaporation temperature, in K.
T_A	is the temperature in the Absorber (absorption temperature), in K.
T_C	is the condensation temperature, in K.
T_G	is the temperature in the Generator (generator temperature), in K.

T_X	is the reference temperature, in K.
$T_{c,1}$; $T_{c,2}$	is the supply and return temperature of chilled water, in K.
$T_{g,1}$; $T_{g,2}$	is the temperature of heating water entering and leaving the Generator, in K.
$T_{h,1}$; $T_{h,2}$	is the supply and return temperature of cooling water, in K.
β	is the Thermo-Chemical Performance Index.
σ_A	is the Quality Loss Index (absorption chiller).
δ_A	is the Coefficient of Compensation for Entropy-Surplus (absorption machine), in K^{-1}.
γ	is the Heat Fraction Factor.
μ_C	is the Thermo-Chemical Instability Index (cooling mode).
λ_C	is the Extreme Values Proximity Index (cooling mode).
COP_C	is the Coefficient of Performance (cooling mode).
$COP_{min,C}$	is the value of Coefficient of Performance (cooling mode) when β=0.
COP_{CC}	is the maximum value of Coefficient of Performance (cooling mode).
COP_H	is the Coefficient of Performance (heating mode).
$\eta_{ex,C}$	is the Exergetic Efficiency (cooling mode), in %.
$\eta_{Ex,min,C}$	is the value of the Exergetic Efficiency (cooling mode) when β=0, in %.
$\eta_{ex,max,C}$	is the value of the Exergetic Efficiency (cooling mode) when COP_C=COP_{CC}, in %.
$\eta_{ex,H}$	is the Exergetic Efficiency (heating mode), in %.
$\eta_{A,C}$	is the Thermo-Chemical Efficiency (cooling mode), in %.
$\eta_{A,min,C}$	is the value of the Thermo-Chemical Efficiency (cooling mode) when β=0, in %.
$\eta_{A,ex,C}$	is the Exergetic Thermo-Chemical Efficiency (cooling mode), in %.
$\eta_{A,ex,min,C}$	is the value of the Exergetic Thermo-Chemical Efficiency (cooling mode) when β=0, in %.

References

1. Santamouris, M. Cooling the buildings—Past, present and future. *Energy Build.* **2016**, *128*, 617–638. https://doi.org/10.1016/j.enbuild.2016.07.034.
2. Csáky, I. Analysis of daily energy demand for cooling in buildings with different comfort categories—Case study. *Energies* **2021**, *14*, 4694. https://doi.org/10.3390/en14154694.
3. Kalmár, F.; Kalmár, T. Thermal comfort aspects of solar gains during the heating season. *Energies* **2020**, *13*, 1702. https://doi.org/10.3390/en13071702.
4. European Commission. *Energy—Roadmap 2050*; Publications Office: Brussels, Belgium, 2012.
5. Kostyák, A.; Szekeres, S.; Csáky, I. Investigation of Sensible Cooling Performance in the Case of an Air Handling Unit System with Indirect Evaporative Cooling: Indirect Evaporative Cooling Effects for the Additional Cooling System of Buildings. *Buildings* **2023**, *13*, 1800. https://doi.org/10.3390/buildings13071800.
6. Nemogne, R.L.F.; Wouagfack, P.A.N.; Nouadje, B.A.M.; Tchinda, R. Exergetic, ecological and thermo-economic (3E) optimization of an absorption heat pump with heat resistance, heat leakage and two internal irreversibilities: Comparison. *Int. J. Refrig.* **2020**, *112*, 251–261. https://doi.org/10.1016/j.ijrefrig.2019.12.016.
7. Kalmár, T.; Szodrai, F.; Kalmár, F. Experimental study of local effectiveness in the case of balanced mechanical ventilation in small offices. *Energy* **2022**, *244*, 122619. https://doi.org/10.1016/j.energy.2021.122619.
8. Kalmár, F.; Kalmár, T. Numerical evaluation of thermal discomfort in conditions of surface heating and asymmetric radiation. *Int. Rev. Appl. Sci. Eng.* **2019**, *9*, 175–179. https://doi.org/10.1556/1848.2018.9.2.14.
9. Wouagfack, P.A.N.; Tchinda, R. Finite-time thermodynamics optimization of absorption refrigeration systems: A review. *Renew. Sustain. Energy Rev.* **2013**, *21*, 524–536. https://doi.org/10.1016/J.RSER.2012.12.015.
10. Feidt, M. Evolution of thermodynamic modelling for three and four heat reservoirs reverse cycle machines: A review and new trends. *Int. J. Refrig.* **2013**, *36*, 8–23. https://doi.org/10.1016/J.IJREFRIG.2012.08.010.
11. Alhuyi-Nazari, M.; Mukhtar, A.; Yasir, A.S.H.M.; Ahmadi, M.H.; Kumar, R.; Luong, T.N.L. Applications of geothermal sources for absorption chillers as efficient and clean cooling technologies for buildings: A comprehensive review. *J. Build. Eng.* **2024**, *82*, 108340. https://doi.org/10.1016/j.jobe.2023.108340.
12. Ehyaei, M.A.; Ahmadi, A.; El Haj Assad, M.; Rosen, M.A. Investigation of an integrated system combining an Organic Rankine Cycle and absorption chiller driven by geothermal energy: Energy, exergy, and economic analyses and optimization. *J. Clean. Prod.* **2020**, *258*, 120780. https://doi.org/10.1016/J.JCLEPRO.2020.120780.
13. Leveni, M.; Cozzolino, R. Energy, exergy, and cost comparison of Goswami cycle and cascade organic Rankine cycle/absorption chiller system for geothermal application. *Energy Convers. Manag.* **2021**, *227*, 113598. https://doi.org/10.1016/J.ENCONMAN.2020.113598.
14. Er, D.; Göktun, S. Optimum performance of an irreversible solar-driven cogeneration heat pump system. *Energy Convers. Manag.* **2001**, *42*, 329–337. https://doi.org/10.1016/S0196-8904(00)00058-3.
15. De Francisco, A.; et al. Development and testing of a prototype of low-power water–ammonia absorption equipment for solar energy applications. *Renew. Energy* **2002**, *25*, 537–544. https://doi.org/10.1016/S0960-1481(01)00093-3.

16. Chahbani, M.H.; Labidi, J.; Paris, J. Modeling of adsorption heat pumps with heat regeneration. *Appl. Therm. Eng.* **2004**, *24*, 431–447. https://doi.org/10.1016/J.APPLTHERMALENG.2003.08.012.
17. Jeong, S.; Kang, B.H.; Karng, S.W. Dynamic simulation of an absorption heat pump for recovering low grade waste heat. *Appl. Therm. Eng.* **1998**, *18*, 1–12. https://doi.org/10.1016/S1359-4311(97)00040-9.
18. Míšek, P.; Adamovský, R.; Neuberger, P. Laboratory and operational analysis of air to water gas absorption heat pump cycle. *Energy Build.* **2023**, *292*, 113180. https://doi.org/10.1016/j.enbuild.2023.113180.
19. Zhang, X.; Wu, J.; Li, Z. Irreversibility characterization and analysis of coupled heat and mass transfer processes in an absorption system. *Int. J. Heat Mass Transf.* **2019**, *133*, 1121–1133. https://doi.org/10.1016/j.ijheatmasstransfer.2019.01.003.
20. Shirazi, A.; Taylor, R.A.; Morrison, G.L.; White, S.D. Solar-powered absorption chillers: A comprehensive and critical review. *Energy Convers. Manag.* **2018**, *171*, 59–81. https://doi.org/10.1016/j.enconman.2018.05.091.
21. Siddiqui, M.U.; Said, S.A.M. A review of solar powered absorption systems. *Renew. Sustain. Energy Rev.* **2015**, *42*, 93–115. https://doi.org/10.1016/J.RSER.2014.10.014.
22. Kim, D.S.; Ferreira, C.A.I. Solar refrigeration options—A state-of-the-art review. *Int. J. Refrig.* **2008**, *31*, 3–15. https://doi.org/10.1016/J.IJREFRIG.2007.07.011.
23. Trutassanawin, S.; Groll, E.A.; Garimella, S.V.; Cremaschi, L. Experimental investigation of a miniature-scale refrigeration system for electronics cooling. *IEEE Trans. Compon. Packag. Technol.* **2006**, *29*, 678–687. https://doi.org/10.1109/TCAPT.2006.881762.
24. Konovalov, D.; Tolstorebrov, I.; Iwamoto, Y.; Kobalava, H.; Lamb, J.J.; Eikevik, T.M. Optimizing Low-Temperature Three-Circuit Evaporative Cooling System for an Electric Motor by Using Refrigerants. *Energies* **2024**, *17*, 3942. https://doi.org/10.3390/en17163942.
25. Manu, S.; Chandrashekar, T.K. A simulation study on performance evaluation of single-stage LiBr–H2O vapor absorption heat pump for chip cooling. *Int. J. Sustain. Built Environ.* **2016**, *5*, 370–386. https://doi.org/10.1016/j.ijsbe.2016.08.002.
26. Chiriac, V.; Chiriac, F. Absorption refrigeration method with alternative water-ammonia solution circulation system for microelectronics cooling. In Proceedings of the 2010 12th IEEE Intersociety Conference on Thermal and Thermomechanical Phenomena in Electronic Systems, ITherm 2010, Las Vegas, NV, USA, 2–5 June 2010; pp. 1–8. https://doi.org/10.1109/ITHERM.2010.5501391.
27. Wu, W.; Wang, B.; Shi, W.; Li, X. Absorption heating technologies: A review and perspective. *Appl. Energy* **2014**, *130*, 51–71. https://doi.org/10.1016/J.APENERGY.2014.05.027.
28. Yang, B.; Jiang, Y.; Fu, L.; Zhang, S. Experimental and theoretical investigation of a novel full-open absorption heat pump applied to district heating by recovering waste heat of flue gas. *Energy Build.* **2018**, *173*, 45–57. https://doi.org/10.1016/J.ENBUILD.2018.05.021.
29. Toghyani, S.; Afshari, E.; Baniasadi, E.; Shadloo, M.S. Energy and exergy analyses of a nanofluid based solar cooling and hydrogen production combined system. *Renew. Energy* **2019**, *141*, 1013–1025. https://doi.org/10.1016/j.renene.2019.04.073.
30. Liu, F.; Dong, F.; Li, Y.; Jia, L. Study on the heating performance and optimal intermediate temperature of a series gas engine compression-absorption heat pump system. *Appl. Therm. Eng.* **2018**, *135*, 34–40. https://doi.org/10.1016/j.applthermaleng.2018.02.010.
31. Le Lostec, B.; Galanis, N.; Millette, J. Experimental study of an ammonia-water absorption chiller. *Int. J. Refrig.* **2012**, *35*, 2275–2286. https://doi.org/10.1016/j.ijrefrig.2012.05.012.
32. Yi, Y.; Xie, X.; Zhang, H.; Jiang, Y. Thermodynamics and process studies on absorption cycle from the perspective of real solution with non-volatile solute. *Energy* **2024**, *291*, 130356. https://doi.org/10.1016/j.energy.2024.130356.
33. Zhao, T.; Chen, X.; Chen, Q. Heat current method-based modeling and optimization of the single effect lithium bromide absorption chiller. *Appl. Therm. Eng.* **2020**, *175*, 115345. https://doi.org/10.1016/j.applthermaleng.2020.115345.
34. Chen, Y.; Han, W.; Jin, H. Thermodynamic performance optimization of the absorption-generation process in an absorption refrigeration cycle. *Energy Convers. Manag.* **2016**, *126*, 290–301. https://doi.org/10.1016/j.enconman.2016.07.086.
35. Bhardwaj, P.K.; Kaushik, S.C.; Jain, S. Finite time optimization of an endoreversible and irreversible vapour absorption refrigeration system. *Energy Convers. Manag.* **2003**, *44*, 1131–1144. https://doi.org/10.1016/S0196-8904(02)00101-2.
36. Su, H.; Gong, G.; Wang, C.; Zhang, Y. Thermodynamic optimization of an irreversible Carnot refrigerator with heat recovery reservoir. *Appl. Therm. Eng.* **2017**, *110*, 1624–1634. https://doi.org/10.1016/J.APPLTHERMALENG.2016.09.013.
37. Bhardwaj, P.K.; Kaushik, S.C.; Jain, S. General performance characteristics of an irreversible vapour absorption refrigeration system using finite time thermodynamic approach. *Int. J. Therm. Sci.* **2005**, *44*, 189–196. https://doi.org/10.1016/J.IJTHERMALSCI.2004.07.004.
38. Qin, X.; Chen, L.; Ge, Y.; Sun, F. Thermodynamic modeling and performance analysis of the variable-temperature heat reservoir absorption heat pump cycle. *Phys. A Stat. Mech. Its Appl.* **2015**, *436*, 788–797. https://doi.org/10.1016/J.PHYSA.2015.05.081.
39. Cardoso-Fernández, V.; Bassam, A.; Tzuc, O.M.; Ch, M.A.B.; de Jesús Chan-González, J.; Soberanis, M.A.E.; Velázquez-Limón, N.; Ricalde, L.J. Global sensitivity analysis of a generator-absorber heat exchange (GAX) system's thermal performance with a hybrid energy source: An approach using artificial intelligence models. *Appl. Therm. Eng.* **2023**, *218*, 119363. https://doi.org/10.1016/J.APPLTHERMALENG.2022.119363.
40. Fumagalli, M.; Sivieri, A.; Aprile, M.; Motta, M.; Zanchi, M. Monitoring of gas driven absorption heat pumps and comparing energy efficiency on primary energy. *Renew. Energy* **2017**, *110*, 115–125. https://doi.org/10.1016/J.RENENE.2016.12.058.

41. Browne, M.W.; Bansal, P.K. Transient simulation of vapour-compression packaged liquid chillers. *Int. J. Refrig.* **2002**, *25*, 597–610. https://doi.org/10.1016/S0140-7007(01)00060-3.
42. Szabó, G.L. *Energy and Exergy Analysis of Radiant Cooling Systems in Buildings*; University of Debrecen: Debrecen, Hungary, 2020.
43. Szabó, G.L. Thermo-chemical instability and energy analysis of absorption heat pumps. *Energies* **2020**, *13*, 1966. https://doi.org/10.3390/en13081966.
44. Szabó, G.L. Exergetic optimization of absorption chillers—A case study. *Case Stud. Therm. Eng.* **2021**, *28*, 101634. https://doi.org/10.1016/j.csite.2021.101634.
45. Szabó, G.L. Energetic and exergetic study of a potential interconnection of a natural gas engine, heat pumps with a thermal and a mechanical compressor. *Therm. Sci. Eng. Prog.* **2022**, *36*, 101525. https://doi.org/10.1016/j.tsep.2022.101525.
46. Arora, C.P. *Refrigeration and Air Conditioning*, 3rd ed.; Tata McGraw-Hill Education Pvt. Ltd.: New Delhi, India, 2009.
47. Balmer, R.T. *Modern Engineering Thermodynamics*; Elsevier Inc.: Amsterdam, The Netherlands, 2011
48. Szabó, G.L. Az abszorpciós gépek jelzőszámai és ezek kapcsolata. *Energiagazdálkodás* **2018**, *59*, 38–42.